Loss function of tumor suppressor FRMD8 confers resistance to tamoxifen therapy via a dual mechanism

Weijie Wu[1#], Miao Yu[1#], Qianchen Li[1], Yiqian Zhao[1], Lei Zhang[1], Yi Sun[1], Zhenbin Wang[1], Yuqing Gong[1], Wenjing Wang[2], Chenying Liu[3], Jing Zhang[1], Yan Tang[1], Xiaojie Xu[4]*, Xiaojing Guo[3]*; Jun Zhan[1]*, Hongquan Zhang[1]*

[1]Program for Cancer and Cell Biology, Department of Human Anatomy, Histology and Embryology, School of Basic Medical Sciences; Peking University International Cancer Institute; and State Key Laboratory of Molecular Oncology, Peking University Health Science Center, Beijing 100191, China.

[2]Department of Gastroenterology, Beijing Friendship Hospital, Capital Medical University; State Key Laboratory for Digestive Health; National Clinical Research Center for Digestive Diseases，Beijing 100050, China.

[3]Department of Breast Pathology and Lab; Tianjin Medical University Cancer Institute & Hospital; National Clinical Research Center for Cancer; Key Laboratory of Breast Cancer Prevention and Therapy of Ministry of Education of China, Tianjin Medical University; Tianjin's Clinical Research Center for Cancer, Tianjin 300060, China.

[4]Department of Genetic Engineering, Beijing Institute of Biotechnology, Beijing 100071, China.

# These two authors contributed equally to this study.

Running title: Loss of FRMD8 downregulates ERα level

Word number of texts: 7,239

Characters with space: 49,894

* Corresponding authors

Hongquan Zhang, Ph.D.; Professor
Peking University Health Science Center,
#38 Xue Yuan Road, Haidian District, Beijing 100191, China.
Tel: 008610-82802424, E-mail: Hongquan.Zhang@bjmu.edu.cn
Or
Jun Zhan, M.D. & Ph.D.; Associate Professor
Peking University Health Science Center,
#38 Xue Yuan Road, Haidian District, Beijing 100191, China.
E-mail: Zhanjun@bjmu.edu.cn

36 Or
37 Xiaojing Guo, M.D. & Ph.D.
38 Tianjin Medical University Cancer Institute & Hospital,
39 West Huanhu Road, Tianjin 300060, China.
40 E-mail: guoxiaojing@tjmuch.com
41 Or
42 Xiaojie Xu, M.D. & Ph.D.; Associate Professor
43 Department of Genetic Engineering, Beijing Institute of Biotechnology,
44 Beijing 100071, China.
45 E-mail: miraclexxj@126.com
46
47

Impact Statement

Tumor suppressive protein FRMD8 inhibits breast cancer progression by regulating the level of ERα and has the possibility to be a potential target for overcoming tamoxifen treatment resistance.

Abstract

Approximately 40% ERα-positive breast cancer patients suffer from therapeutic resistance to tamoxifen. Although reduced ERα level is the major cause of tamoxifen resistance, the underlying mechanisms remain elusive. Here, we report that FRMD8 raises the level of ERα at both transcriptional and post-translational layers. FRMD8 deficiency in *MMTV-Cre*$^{+}$; *Frmd8*$^{fl/fl}$; *PyMT* mice accelerates mammary tumor growth and loss of luminal phenotype, and confers tamoxifen resistance. Single-cell RNA profiling reveals that Frmd8 loss decreases the proportion of hormone-sensing differentiated epithelial cells and downregulates the levels of ERα. Mechanically, on one hand, loss of FRMD8 inhibits *ESR1* transcription via suppressing the expression of FOXO3A, a transcription factor of *ESR1*. On the other hand, FRMD8 interacts both with ERα and UBE3A, and disrupts the interaction of UBE3A with ERα, thereby blocking UBE3A-mediated ERα degradation. In breast cancer patients, *FRMD8* gene promoter is found hypermethylated and low level of FRMD8 predicts poor prognosis. Therefore, FRMD8 is an important regulator of ERα and may control therapeutic sensitivity to tamoxifen in ERα-positive breast cancer patients.

Keywords: FRMD8; Breast cancer; ERα; Tamoxifen resistance; UBE3A

Introduction

Breast cancer is the most commonly diagnosed cancer worldwide(Sung et al., 2021) and more than 70% of breast cancer are estrogen receptor α (ERα)-positive(Habara & Shimada, 2022). Although endocrine therapy is the most common systemic treatment for ERα-positive breast cancer in clinical practice, approximately 40% of patients still develop primary or secondary resistance to endocrine therapy(Badia et al., 2007; Légaré & Basik, 2016; Rondón-Lagos et al., 2016). Therefore, it is urgent and necessary to explore the mechanisms of endocrine therapy resistance and search for new therapeutic targets.

ERα is a ligand-activated transcription factor that is activated by oestrogen, and promotes cell proliferation during breast cancer development (Harbeck et al., 2019). Tamoxifen (TAM), a selective estrogen receptor antagonist, is the most widely used medicine in endocrine therapy. Tamoxifen competes with estrogen to bind with ERα and changes the conformation of ERα, thereby preventing the interaction between co-activators and ERα and inhibiting activation of ERα (Katzenellenbogen et al., 2018). Thus, the level of ERα is strongly correlated with reactivity and resistance of endocrine therapy. Uncovering the mechanisms by which ERα expression is regulated is essential for overcoming endocrine therapy resistance. Multiple transcription factors, such as AP-2γ, FOXO3, FOXM1, and GATA3, have been reported to bind to the promoter region of *ESR1*, the gene encoding ERα, and participate in transcriptional regulation of *ESR1*(Jia et al., 2019; Koš et al., 2001). In addition, post-translational modifications of ERα, including phosphorylation, acetylation, and ubiquitination, also have effects on subcellular localization, transcriptional activity, and stability of ERα(Rogatsky et al., 1999; Williams et al., 2009; Zhou & Slingerland, 2014). However, the mechanisms underlying the regulation of ERα expression are still not clear and require further investigation.

FERM domain-containing proteins are widely involved in processes such as the formation of macromolecular complexes, subcellular localization, functional activation,

101 and signal transduction, thereby regulating the occurrence and development of
102 tumors(Frame et al., 2010; Moleirinho et al., 2013; Zhan & Zhang, 2018). FRMD8, as
103 a member of FERM domain-containing proteins, has been reported to bind with iRhom
104 and enhance the stability of the iRhom/TACE complex on the cell surface, thereby
105 preventing iRhom/TACE degradation mediated by lysosomes. TACE is responsible for
106 cleaving and releasing TNF, and the absence of FRMD8 impairs the production of
107 TNF(Künzel et al., 2018; Oikonomidi et al., 2018). Additionally, FRMD8 expressions
108 in both microenvironment and tumor cells promote lung tumor growth(Badenes et al.,
109 2023). FRMD8 inhibits colon cancer growth by preventing cell cycle progression.
110 FRMD8 disrupts the interaction of CDK7 with CDK4, subsequently inhibiting CDK4
111 activation. Furthermore, FRMD8 competes with MDM2 to bind RB, thereby
112 attenuating MDM2-mediated RB degradation(Yu et al., 2023). However, the roles of
113 FRMD8 in breast tumorigenesis and progression need further exploration.
114 In this study, we found that loss of Frmd8 in luminal epithelial cells of *MMTV-PyMT*
115 mice accelerates mammary tumor progression and luminal epithelial phenotype loss,
116 and confers tamoxifen resistance. Single-cell RNA profiling reveals that the number of
117 hormone-sensing differentiated cells is diminished and the level of ERα is decreased in
118 Frmd8-knocked-out mammary tumors. FRMD8 not only increases *ESR1* expression,
119 but also prevents ERα degradation by interrupting the interaction between ERα and E3
120 ligase UBE3A. Further, a low FRMD8 level predicts poor prognosis in human breast
121 cancer patients. Thus, we demonstrated that FRMD8 is an important ERα regulator and
122 a vital tumor suppressive protein in breast cancer growth and drug resistance.
123

Results

Loss of Frmd8 promotes mammary tumor growth and generates tamoxifen resistance *in vivo*

To examine whether FRMD8 plays a role in breast tumorigenesis, we established luminal epithelium-specific *Frmd8* knockout mice (*MMTV-Cre*$^{+}$; *Frmd8*$^{fl/fl}$) (Fig. 1A and 1B) and further generated a Frmd8-deletion breast cancer mouse model (*MMTV-Cre*$^{+}$; *Frmd8*$^{fl/fl}$; *PyMT*) by crossing *MMTV-Cre*$^{+}$; *Frmd8*$^{fl/fl}$ mice with *MMTV-PyMT* (*PyMT*) mice, a widely used transgenic mouse model of mammary tumorigenesis (Fig. 1C, 1D, S1A and S1B). Compared with *MMTV-Cre*$^{-}$; *Frmd8*$^{fl/fl}$; *PyMT* mice, Frmd8 depleted in mice significantly promotes mammary tumor development (Fig. 1E and 1F). The total tumor weight (Fig. 1G) and number of tumors (Fig. 1H) were markedly higher in *MMTV-Cre*$^{+}$; *Frmd8*$^{fl/fl}$; *PyMT* mice than the control mice. Histological examination of the breast tumors from *PyMT* mice using haematoxylin-eosin (H&E) staining revealed that the luminal epithelium was poorly differentiated in *MMTV-Cre*$^{+}$; *Frmd8*$^{fl/fl}$; *PyMT* mice tumors compared with the control mice (Fig. 1I). Furthermore, immunohistochemical staining showed that the percentage of Ki67-positive cells was significantly elevated in mammary tumors of *Frmd8*-depleted mice (Fig. 1J and 1K). Consistently, 5-ethynyl-2'-deoxyuridine (EdU) incorporation assays demonstrated that FRMD8 depletion promoted human breast cancer cell MCF7 and T47D proliferation (Fig. S1C and S1D). These findings indicated that *Frmd8* deficiency in the luminal epithelium accelerates mammary tumor growth in *MMTV-PyMT* mice and promotes cell proliferation.

Since tamoxifen is commonly used for the treatment of ERα^{+}/HER2^{-} breast cancer, we thus investigated whether loss of Frmd8 affects sensitivity of mammary tumors to tamoxifen treatment in mice. To this end, *MMTV-Cre*$^{-}$; *Frmd8*$^{fl/fl}$; *PyMT* mice and *MMTV-Cre*$^{+}$; *Frmd8*$^{fl/fl}$; *PyMT* mice were injected intraperitoneally with tamoxifen or corn oil as control every two days. The results showed that tamoxifen significantly prevents mammary tumor progression in the control mice (Fig. 1L and 1M). However,

152 mammary tumors of *MMTV-Cre*$^{+}$; *Frmd8*$^{fl/fl}$; *PyMT* mice showed no response to
153 tamoxifen treatment (Fig. 1L and 1M). Consistently, the total tumor weight (Fig. 1N)
154 and number of tumors (Fig. 1O) of *MMTV-Cre*$^{-}$; *Frmd8*$^{fl/fl}$; *PyMT* mice were markedly
155 decreased after tamoxifen treatment, whereas there was no difference in *MMTV-Cre*$^{+}$;
156 *Frmd8*$^{fl/fl}$; *PyMT* mice (Fig. 1N and 1O). Taken together, these findings demonstrated
157 that loss of Frmd8 accelerates mammary tumor growth and generates resistance to
158 tamoxifen therapy in Frmd8-depleted mice.
159

160 **Frmd8 knockout decreases the proportion of the hormone-sensing differentiated**
161 **epithelial cells**

162 To investigate the mechanism through which Frmd8 loss promotes mammary tumor
163 growth and leads to tamoxifen resistance, we then performed single-cell RNA
164 sequencing (scRNA-seq) analysis. Mammary tumors from 4-month-old *MMTV-Cre*$^{-}$;
165 *Frmd8*$^{fl/fl}$; *PyMT* and *MMTV-Cre*$^{+}$; *Frmd8*$^{fl/fl}$; *PyMT* mice were harvested and analyzed
166 using the Chromium Single Cell 3' Reagent Kitsv3 (10× Genomics). Cells that passed
167 quality control (QC) filter totaled 24,320, of which 11,606 cells were from *MMTV-Cre*$^{-}$;
168 *Frmd8*$^{fl/fl}$; *PyMT*, and 12,714 cells were from *MMTV -Cre*$^{+}$; *Frmd8*$^{fl/fl}$; *PyMT* mice (Fig.
169 2A). After that, we profiled the three major cell lineages, including epithelial cells,
170 immune cells and stromal cells by the UMAP visualization (Fig. 2B). Their associated
171 top-expressed and canonical markers were shown in Figure S2A and S2B, respectively.
172 Based on the expression of known markers, a total of 12 clearly separated cell lineages
173 were finally identified (Fig. 2C and 2D). In particular, they were as follows: B cells
174 highly expressing *Cd19*, *Cd79a*, *Cd79b*; CD4^{+} T cells characterized with high *Cd3g*
175 and *Cd4* expression; CD8^{+} T cells highly expressing *Cd3g* and *Cd8a*; dendritic cells
176 (DCs) expressing *Cd74* and *Cd14*; endothelial cells specifically expressing the markers
177 *Pecam1* and *Emcn*; epithelial cells expressing *Epcam* and *Krt8*; fibroblast cells high
178 expressing *Col1a1* and *Col3a1*; granulocyte cells specifically expressing the markers
179 *S100a9*; macrophage cells highly expressing *Cd14*, *Cd68* and *C1qa*; monocyte cells

180 highly expressing *Cd14* and *Ccr2*; natural killer (NK) cells specifically expressing
181 *Nkg7* and *Ncr1* (Fig. S2C). The dot plots compared the proportion of cells expressing
182 cluster-specific markers and their scaled relative expression levels (Fig. S2D).
183 To further explore whether the proportions of epithelial cells in mammary tumors
184 were affected by Frmd8 loss, we subset and re-identified four epithelial cell
185 clusters(Valdes-Mora et al., 2021), including alveolar progenitor (Avp), basal (Bsl),
186 hormone-sensing differentiated (Hsd) and luminal progenitor (Lp) epithelial cells (Fig.
187 2E). As expected, the epithelial cells were composed of luminal epithelial cells and
188 basal epithelial cells, which were consistent with the cellular characteristics of the
189 mammary glands. In contrast to control mice, the proportion of the Hsd epithelial cells
190 was significantly decreased in *MMTV-Cre*$^{+}$; *Frmd8*$^{fl/fl}$; *PyMT* mice (Fig. 2F).
191 To define the tumor cells in the mouse mammary tumors, we applied inferCNV
192 algorithm to calculate the copy number variations (CNVs) of the single cells (Fig. 2G).
193 To this end, we analyzed CNV scores of epithelial subclusters, immune and stromal
194 cells, revealing immune cells with low CNV score (Fig. 2H). Given that Hsd epithelial
195 cells which specifically expressed *Esr1* and *Pgr* had lower CNV score than alveolar
196 progenitor (Avp), basal (Bsl) and luminal progenitor (Lp) epithelial cells, we defined
197 the low CNV score Hsd epithelial cells as normal cells (Fig. 2H and 2I). Furthermore,
198 we defined the high CNV score epithelial cells as tumor cells, and plotted the UMAP
199 visualization (Fig. 2J). The results also showed that the expression of *Frmd8* was
200 decreased in tumor cells compared with normal cells (Fig. 2K and S2E). In addition,
201 we observed that loss of Frmd8 significantly decreased the expression of *Esr1* and *Pgr*
202 in normal cells of mammary tumors, and decreased expression of Frmd8 in tumor cells
203 accompanied with low expression of *Esr1* and *Pgr* compared with normal cells (Fig.
204 2L and S2E). Taken together, these findings indicated that Frmd8 depletion in *PyMT*
205 mice leads to decreases of the Hsd epithelial cells proportion and the expression of *Esr1*
206 and *Pgr*.
207

208 **FRMD8 promotion of *ESR1* expression is mediated by FOXO3A**

209 Given that scRNA-seq results suggested that loss of Frmd8 reduced the proportion of
210 Hsd epithelial cells and the expression of *Esr1* and *Pgr*, multiple immunofluorescence
211 staining analyses were then performed to examine the change of ERα and PR at the
212 protein levels *in situ* in mammary tumors of 4-month-old Frmd8-depleted mice.
213 Consistent with the scRNA-seq results, deficiency of Frmd8 dramatically decreased the
214 levels of ERα, PR and CK8, a marker of mammary luminal epithelium, in normal
215 tissues adjacent to tumors (Fig. 3A and 3B). *In situ* tissue flow cytometry analysis
216 demonstrated that in normal tissues adjacent to tumor of the control mice, the
217 proportion of ERα-positive cells among $CK8^{+}$ cells were 45.49%, whereas this
218 proportion was just 9.28% in *MMTV-Cre*$^{+}$; *Frmd8*$^{fl/fl}$; *PyMT* mice (Fig. S3A). Similarly,
219 the proportion of PR-positive cells among $CK8^{+}$ cells was also reduced in normal
220 tissues adjacent to tumor of *MMTV-Cre*$^{+}$; *Frmd8*$^{fl/fl}$; *PyMT* mice compared with the
221 control mice (Fig. S3B). $FRMD8^{high}ER\alpha^{high}$ and $FRMD8^{high}PR^{high}$ cells were mainly
222 present in normal tissues adjacent to tumor of *MMTV-Cre*$^{-}$; *Frmd8*$^{fl/fl}$; *PyMT* mice,
223 whereas Frmd8 depletion led to $FRMD8^{low}ER\alpha^{low}$ and $FRMD8^{low}PR^{low}$ cells markedly
224 increased (Fig. S3C and S3D). In mammary tumor tissues from both control mice and
225 *MMTV-Cre*$^{+}$; *Frmd8*$^{fl/fl}$; *PyMT* mice, the expressions of ERα and PR were almost
226 negative (Fig. 3A and 3B). Since the expression of ERα is loss with tumor progression,
227 to further clarify the regulation of Frmd8 on ERα, we performed immunohistochemistry
228 (IHC) staining of mammary glands of 7-week-old *PyMT* mice, which had no palpable
229 tumors. The results showed that Frmd8 depletion also markedly decreased the
230 expression of ERα in normal and atypical hyperplasia breast tissues (Fig. S3E). Taken
231 together, these data suggested that deficiency of FRMD8 downregulates the protein
232 levels of ERα and PR in mammary tissues of *MMTV-PyMT* mice, and accelerates the
233 loss of luminal phenotype in mammary gland.

234 It was known that the common endocrine treatment for non-metastatic breast cancer
235 relies on the expression of ERα(Waks & Winer, 2019) and our results demonstrated that

236 loss of Frmd8 promotes mammary tumor growth and confers tamoxifen resistance in
237 mice, we thus aim to further examine whether FRMD8 regulates ERα expression. To
238 this end, we transiently transfect Flag-FRMD8 vector or FRMD8 siRNA in human
239 breast cancer cells. Our results showed that FRMD8 overexpression drastically
240 increased the levels of ERα, while ERα expression was greatly downregulated when
241 FRMD8 was knocked down (Fig. 3C and 3D). Moreover, qRT-PCR results indicated
242 that depletion of FRMD8 significantly decreased the mRNA level of *ESR1* (Fig. 3E).
243 FOXO3A is a crucial transcription factor for ERα(Jia et al., 2019). To answer whether
244 FOXO3A is involved in the regulation of FRMD8 on ERα, we examined the expression
245 of FOXO3A after silencing FRMD8 through transfecting siRNA into MCF7 and T47D
246 cells. The results showed that FRMD8 silencing dramatically decreased the level of
247 FOXO3A (Fig. 3F). Consistently, overexpression of FRMD8 in MCF7 and T47D cells
248 markedly raised the level of FOXO3A (Fig. 3G). To examine whether FRMD8
249 promotes *ESR1* transcription through FOXO3A, HA-tagged FRMD8 as well as
250 FOXO3A siRNA were co-transfected into MCF7 cells. Although exogenous FRMD8
251 significantly upregulated ERα expression, depletion of endogenous FOXO3A greatly
252 reduced the effect of FRMD8 on ERα (Fig. 3H and 3I). Besides, chromatin
253 immunoprecipitation (ChIP)-qPCR was performed and revealed that depletion of
254 FRMD8 significantly decreased the occupancy of FOXO3A at the *ESR1* promoters (Fig.
255 3J). Altogether, these data indicated that FRMD8 promoted upregulation of *ESR1* is
256 mediated by FOXO3A (Fig. 3K).
257
258 **FRMD8 stabilizes ERα via prevention of its degradation**
259 Although our results suggest that FRMD8 depletion inhibits the mRNA level of *ESR1*,
260 unexpectedly, we also observed that decreased expression of FRMD8 led to a decreased
261 level of exogenous Flag-ERα (Fig. 4A). This result suggested that in addition to
262 inhibiting mRNA expression of ERα, FRMD8 may also regulate ERα protein
263 expression at the post-translational level. To this end, T47D cells were treated with

264 cycloheximide (CHX), a protein synthesis inhibitor. Depletion of FRMD8 greatly
265 increased the ERα turnover rate and the half-life of ERα decreased from 6 h to
266 approximately 2 h (Fig. 4B and 4C). Furthermore, MCF7 and T47D cells were treated
267 with MG132, a proteasome inhibitor, and chloroquine (CQ), a lysosome inhibitor, to
268 determine whether ERα degradation was mediated by the proteasome or the lysosome.
269 The results showed that the reduction of ERα levels by FRMD8 depletion was blocked
270 by treatment with MG132 but not CQ (Fig 4D). Altogether, these data suggested that
271 FRMD8 stabilizes ERα protein via a proteasome-mediated degradation pathway.
272
273 **FRMD8 inhibits ERα degradation by blocking UBE3A binding with ERα**
274 Given that FERM domain containing proteins play roles via regulating protein-protein
275 interaction, we wonder whether there is an interaction between FRMD8 and ERα. To
276 this end, co-immunoprecipitation (co-IP) assays were performed using Flag-FRMD8 in
277 MCF7 and T47D cells to examine the association of exogenous FRMD8 with
278 endogenous ERα. The results showed that FRMD8 interacts with ERα (Fig. 5A and 5B).
279 Importantly, an interaction between endogenous FRMD8 and endogenous ERα was
280 also observed in MCF7 cells (Fig. 5C). Furthermore, a glutathione S-transferase (GST)
281 pull-down assay using purified recombinant GST-FRMD8 and Flag-tagged ERα
282 proteins was also performed. The results indicated that FRMD8 interacts directly with
283 ERα *in vitro* (Fig. 5D). Taken together, these findings suggest that FRMD8 is a binding
284 partner of ERα in human cells.
285 The aforementioned findings demonstrated that FRMD8 prevents ERα degradation
286 via proteasome pathway. To explore the mechanism by which FRMD8 inhibits ERα
287 degradation, co-IP assay and mass spectrometry (MS) analysis were performed in
288 HEK293A cells transiently expressing Flag-FRMD8 (Table S1). We next searched for
289 the FRMD8-interacting proteins identified by MS matched with the known E3 ubiquitin
290 ligases of ERα. Interestingly, UBE3A, a ubiquitin ligase for ERα(Sun et al., 2012), is
291 the only matched protein that interacts with FRMD8 (Fig. 5E). We thus examined the

292 interaction between FRMD8 and UBE3A through co-IP. The results indicated an
293 interaction between FRMD8 and UBE3A (Fig. 5F and 5G). Further, we assumed that
294 FRMD8 may interfere with the interaction between ERα and UBE3A. To test this idea,
295 co-IP assays were performed in HEK293T and T47D cells. In both cell types, the level
296 of ERα ubiquitination and the interaction between ERα and UBE3A were markedly
297 increased by FRMD8 depletion (Fig. 5H and 5I). Intriguingly, FRMD8 depletion led to
298 a marked decrease of ERα expression, while depletion of UBE3A dramatically rescued
299 the effect of FRMD8 depletion (Fig. 5J and 5K). Taken together, these results strongly
300 demonstrated that FRMD8 binds to ERα and UBE3A, and prevents UBE3A interaction
301 with ERα, thereby blocking UBE3A-mediated ERα ubiquitination and degradation (Fig.
302 5L).
303

304 ***FRMD8* promoter is methylated and low FRMD8 level predicts poor prognosis in**
305 **breast cancer patients**

306 Given that Frmd8 prevents mammary tumor growth and inhibits tumor cell
307 proliferation in mice (Fig. 1), we would like to investigate whether the expression of
308 FRMD8 is downregulated in mammary tumors. ScRNA-seq results demonstrated that
309 the level of *Frmd8* in normal Hsd epithelial cells was significantly higher than other
310 tumor cells in the mammary tumors from *PyMT* mice (Fig. 6A). To further verify the
311 expression of FRMD8 in human breast cancer cell lines, whole cell lysates from normal
312 mammary epithelial cells and various subtypes of breast cancer cell lines were
313 subjected to Western blot analysis. Results showed that FRMD8 expression was lower
314 in claudin-low breast cancer cell lines compared with normal mammary epithelial cell
315 line or ERα-positive cell lines (Fig. 6B).

316 Hypermethylation of tumor suppressor genes is one of the major causes for
317 tumorigenesis. Therefore, we investigated whether the promoter region of FRMD8 is
318 hypermethylated in breast cancer patients. An analysis based on TCGA database
319 showed that the *FRMD8* promoter was highly methylated in primary breast tumors (Fig.

320 6C). Subsequently, breast cancer cells were treated with the DNA methyltransferase
321 inhibitor 5-aza-2-deoxycytidine (5-Aza-dC). The results showed that 5-Aza-dC
322 treatment significantly upregulated both mRNA and protein levels of FRMD8 in
323 claudin-low but not luminal breast cancer cell lines (Fig. 6D, 6E and S4A), which was
324 consistent with the lower expression of FRMD8 in claudin-low breast cancer cell lines
325 (Fig. 6A). These findings demonstrated that *FRMD8* gene promoter is hypermethylated,
326 which could be the reason for the reduced FRMD8 expression in triple-negative breast
327 cancer cells.

328 To further investigate the clinical significance of FRMD8 in breast cancer patients,
329 we performed immunohistochemical staining of FRMD8 in a tissue microarray of
330 breast cancer patients and evaluated the level of FRMD8 (Fig. 6F). The results
331 suggested that patients with lower level of FRMD8 showed poor overall survival
332 (p=0.0409) (Fig. 6G). Moreover, we also found that a decreased FRMD8 level was
333 associated with poor recurrence free survival in breast cancer patients according to
334 Kaplan-Meier Plotter analysis (Fig. 6H, 6J, S4B and S4C). Collectively, these data
335 indicated that the promoter of *FRMD8* is hypermethylated, and the low FRMD8 level
336 predicts poor prognosis of breast cancer patients.

337

338 **Discussion**

339 In this study, we found that FRMD8 plays a tumor suppressive role in breast cancer
340 progression. We demonstrated that loss of FRMD8 promotes mammary tumor growth,
341 accelerates the loss of mammary luminal phenotype, and confers tamoxifen resistance
342 via downregulating ERα level. FRMD8 depletion not only suppresses transcription of
343 *ESR1* through decreasing the level of FOXO3A, but also promotes the E3 ligase
344 UBE3A binding with ERα to disrupts ERα protein stability. Moreover, the promoter of
345 *FRMD8* is hypermethylated and a decreased FRMD8 level predicts poor outcomes in
346 breast cancer patients (Fig. 7).

347 As a FERM-domain containing protein, FRMD8 is necessary for releasing of TNF

348 and EGFR ligands(Künzel et al., 2018; Oikonomidi et al., 2018). FRMD8 regulates
349 lung cancer cell growth by regulating tumor microenvironment(Badenes et al., 2023).
350 Frmd8-deficient mice are defective in intestinal epithelial barrier repair function and
351 deletion of Frmd8 promotes colorectal tumorigenesis induced by azoxymethane/
352 dextran sodium sulfate in mice(Badenes et al., 2023; Yu et al., 2023). FRMD8 acts as a
353 scaffold protein, inhibiting CDK4 activation mediated by CDK7 and preventing
354 MDM2-mediated RB degradation(Yu et al., 2023). In this study, our results suggested
355 that FRMD8 inhibits mammary tumor progression in *MMTV-PyMT* mice. Besides,
356 FRMD8 also acts as a scaffold molecule, which interacts simultaneously with ERα and
357 UBE3A, and renders UBE3A unable to bind with ERα, thus stabilizing ERα.

358 In *MMTV-PyMT* mice, early-stage mammary tumors express ERα and PR, but these
359 receptors are gradually lost as the tumor progresses (Lapidus et al., 1998). Our scRNA-
360 seq results revealed that mammary tumor epithelial cells in *MMTV-PyMT* mice fall into
361 four clusters, with only Hsd epithelial cells showing ERα and PR expression.
362 Additionally, Hsd epithelial cells exhibited the lowest CNV score, indicating a closer
363 resemblance to normal epithelial cells. The loss of Frmd8 reduced the proportion of
364 Hsd epithelial cells and led to a downregulation of ERα and PR expression, implying
365 that Frmd8 deficiency promotes the loss of luminal features in the mammary gland and
366 accelerates mammary tumor progression.

367 In this study, we identified that loss of FRMD8 inhibiting *ESR1* expression through
368 downregulating the level of FOXO3A. FOXO3A locates in nucleus and blocks cell
369 cycle progression via activating the cell cycle blocking protein $p27^{KIP1}$ (Seoane et al.,
370 2004). In addition, FOXO3A contributes to cell death through a Fas ligand-dependent
371 mechanism(Seoane et al., 2004). Phosphorylated FOXO3A mediated by AKT binds to
372 14-3-3 protein and remains in the cytoplasm, resulting in loss of activity(Arden, 2004).
373 Thus, FRMD8 may also be involved in the regulation of cell cycle or apoptosis in an
374 ERα-independent manner by regulating FOXO3A. Furthermore, FOXO3A is closely
375 associated with the stemness of breast cancer cells. FOXO3A suppresses breast cancer

376 stem cell properties and tumorigenicity via inhibition of FOXM1/SOX2 signaling(Liu
377 et al., 2020; Yan et al., 2017), suggesting that FRMD8 may have an effect on breast
378 cancer stem cells. However, the mechanisms by which FRMD8 promotes FOXO3A
379 expression remain unclear and need to be further investigated.

380 The proportion of luminal subtype is increasing in new cases of breast cancer(Waks
381 & Winer, 2019). Tamoxifen therapy is one of the most important systemic treatment for
382 $ER\alpha^{+}/HER2^{-}$ subtype breast cancer patients(Waks & Winer, 2019). Unfortunately,
383 primary or secondary tamoxifen resistance occurs in about 40% of patients treated with
384 tamoxifen therapy, and tamoxifen resistance often leads to the development of
385 resistance to other selective estrogen receptor modulators(Badia et al., 2007; Légaré &
386 Basik, 2016; Rondón-Lagos et al., 2016). As a regulator of ERα, FRMD8 may be a
387 therapeutic target for rescue tamoxifen resistance.

388 In summary, we identified FRMD8 as a prognostic marker in breast cancer. FRMD8
389 regulates ERα level through a dual mechanism. Loss of FRMD8 inhibits *ESR1*
390 transcription via downregulating FOXO3A expression. FRMD8 also stabilizes ERα
391 protein by preventing UBE3A from binding to ERα. Deficiency of FRMD8 promotes
392 mammary luminal features loss and confers tamoxifen resistance. Our findings
393 indicated that targeting *FRMD8* promoter methylation may provide a novel therapeutic
394 approach for reversing tamoxifen resistance.
395

396 ## Materials and Methods

397 **Mice**

398 Both *Frmd8* floxed mice and *MMTV-PyMT* mice were purchased from Shanghai Model
399 Organisms Center Inc (SMOC). *MMTV-Cre*$^{+}$ mice were from the Nanjing Biomedical
400 Research Institute of Nanjing University.

401 *Frmd8* floxed (*Frmd8*$^{fl/fl}$) mice were crossed with *MMTV-Cre*$^{+}$; *PyMT* transgenic
402 mice to generate *Frmd8* heterozygous (*MMTV-Cre*$^{+}$; *Frmd8*$^{fl/wt}$; *PyMT*) mice. *MMTV-*
403 *Cre*$^{+}$; *Frmd8*$^{fl/wt}$; *PyMT* mice were further backcrossed with *Frmd8*$^{fl/fl}$ mice to obtain
404 littermate *MMTV-Cre*$^{-}$; *Frmd8*$^{fl/fl}$; *PyMT* and *MMTV-Cre*$^{+}$; *Frmd8*$^{fl/fl}$; *PyMT* mice.

405 Mice were housed in a pathogen-free animal facility at Laboratory Animal Center of
406 Peking University Health Science Center with a 12 h light/dark cycle, constant
407 temperature and humidity, and fed standard rodent chow and water ad libitum. All
408 animal experiments were approved by the Peking University Biomedical Ethics
409 Committee and the approval number is BCJB0104. Genomic DNA extracted from
410 mouse tail biopsies was subjected to standard genotyping PCR using the primers
411 specified in Table S3. The reaction conditions were: 5 minutes at 94℃; 35 cycles of 30
412 s at 94℃, 30 s at 56℃ and 1 minute at 72℃; followed by 5 minutes at 72℃ and hold
413 at 4℃.

414

415 **Tamoxifen treatment**

416 7-week-old female mice were given intraperitoneal injections of either corn oil or
417 tamoxifen (50 mg/kg) every two days. Tumor formation was assessed every two days,
418 and the time point at which the tumor first became palpable was recorded as the tumor-
419 free survival time. At the end of the treatment, mice were euthanized and the total
420 number of tumors were counted. Tumors were measured using calipers, and tumor
421 volume was calculated using the formula: V = (length × width × height × 0.5) mm^3.
422 Tumors were subsequently fixed in 4% paraformaldehyde (PFA) and housed in
423 individual cassettes for paraffin embedding. 5 μm sections were stained for

424 hematoxylin-eosin (H&E) or immunohistochemistry.

425

426 **Antibodies and reagents**

427 Antibodies against ERα (#8644), Ubiquitin (#3936) and PR (#8757) were purchased
428 from Cell Signaling Technology. Antibodies specific for ERα (#ab32063), CK8
429 (#ab53280), FOXO3A (#ab109629), UBE3A (#ab272168) and HER2 (#ab134182)
430 were from Abcam. Anti-PR (#YM3348) antibody was from Immunoway. Anti-FRMD8
431 (#HPA002861) antibody was from Atlas Antibodies. Anti-Flag (#F3165) antibody was
432 from Sigma-Aldrich. Antibodies against GAPDH (#AC002) was purchased from
433 ABclonal Technology. Anti-Actin (#sc-58673) antibodies was from Santa Cruz
434 Biotechnology. Antibodies specific for β-tubulin (#TA-10) was from Zhong Shan Jin
435 Qiao (ZSGB-Bio).

436 MG132 (#S2619) was purchased from Selleck. Chloroquine (CQ, #C6628),
437 cycloheximide (#C7698) and 5-aza-2-deoxycytidine (5-Aza-dC; #A3656) were
438 purchased from Sigma-Aldrich. Tamoxifen (#HY-13757A) and estradiol (E2, #HY-
439 B0141) were purchased from MedChemExpress.

440

441 **Plasmids**

442 The recombinant vectors encoding human FRMD8 and ERα were constructed by PCR-
443 based amplification, and then subcloned into the p3×Flag-CMV^{TM}-10 expression vector.
444 The GST-tagged FRMD8 expression plasmid was generated by inserting PCR-
445 amplified fragments into pGEX-4T-1 vector. All constructs were confirmed by DNA
446 sequencing.

447

448 **Cell culture**

449 Human embryonic kidney cell lines HEK293T and HEK293A and human breast cancer
450 cell lines MCF7, BT-20, MDA-MB-231 and SUM159 were cultured in Dulbecco's
451 Modified Eagle Medium (DMEM). Human breast cancer cell lines T47D and BT-549

452 were cultured in RPMI 1640 medium. All media were supplemented with 10% fetal
453 bovine serum, 100 U/ml penicillin and 0.1 mg/ml streptomycin. Medium for culturing
454 T47D was supplemented with 0.2 U/ml insulin. Human breast cancer cell line MCF10A
455 was cultured in DMEM/F12 medium supplemented with 10% horse serum, 100 U/ml
456 penicillin and 0.1 mg/ml streptomycin, 20 ng/ml epidermal growth factor, 0.5 μg/ml
457 hydrocortisone, 10 μg/ml insulin and 100 ng/ml cholera toxin. All cell lines were
458 maintained in a humidified atmosphere at 37°C with 5% CO_2 and passaged using 0.25%
459 trypsin containing 0.02% EDTA for dissociation at 80% confluence.
460
461 **Plasmid and specific siRNA transfection**
462 For transient transfection, cells at 50%-60% confluence were transfected with plasmids
463 via polyethylenimine (PEI; Polyscience, #24765). For RNA interference experiments,
464 cells at 60-70% confluence were transfected with siRNA using Lipo8000 (Beyotime, #
465 C0533). The specific sequences of siRNA are listed in Table S2.
466
467 **Extraction of proteins and immunoblotting**
468 Cells or tissues were lysed using RIPA buffer (1×PBS, pH 7.4, 0.5% sodium
469 deoxycholate, 1% NP-40, and 0.1% SDS) complemented with an EDTA-free cocktail
470 of protease inhibitors (Roche). This was followed by centrifugation at 12,000 rpm for
471 over 15 minutes at a temperature of 4°C to collect the supernatant. Protein
472 concentrations were ascertained using a bicinchoninic acid (BCA) protein assay kit
473 (Applygen, #P1511). Protein samples underwent electrophoresis via SDS-PAGE and
474 were then transferred to a polyvinylidene fluoride (PVDF) membrane employing
475 conventional methods. The membranes were treated with 5% non-fat milk for one hour,
476 then incubated with primary antibodies at 4°C overnight, and subsequently exposed to
477 HRP-conjugated goat anti-mouse or rabbit IgG secondary antibodies for one hour at
478 4°C. The bound antibodies were visualized using the EZ-ECL Chemiluminescence
479 Detection Kit for HRP (Biological Industries, # 20-500-1000) through

480 ChampChemiTM (SageCreation).

481

482 **Chromatin immunoprecipitation**

483 The chromatin immunoprecipitation (ChIP) assay was performed according to the
484 manufacturer's instructions of Sonication ChIP Kit (ABclonal, #RK20258). The
485 purified DNA was analyzed by quantitative reverse transcription PCR (qRT-PCR). All
486 primers are shown in Table S2.

487

488 **Immunoprecipitation**

489 IgG, serving as controls, or indicated antibodies were added to pre-cleared lysates and
490 allowed to incubate overnight at 4°C with sustained rocking. Following this, lysates
491 were subjected to a 4-hour incubation with 35-50 μl of either protein A or protein G
492 Sepharose beads (Santa Cruz Biotechnology) at 4°C. Subsequently, the Sepharose
493 beads were washed thrice with RIPA buffer and heated in SDS-loading buffer at 99°C
494 for 10 minutes. The immunoprecipitation results were assessed via immunoblotting.

495

496 **Mass spectrometry analysis**

497 Flag-FRMD8 and empty vector were transiently transfected in HEK293A cells using
498 PEI, and cell lysates were harvested after 48 h. The cell lysates were pre-cleared and
499 then incubated with pre-washed anti-Flag M2 agarose beads (Yeasen, #20584ES08)
500 overnight at 4°C. Beads were washed three times with PBS. Protein samples were then
501 eluted by boiling with sodium dodecyl sulfate (SDS)-loading buffer at 99°C for 10 min.
502 Ten percent of the samples were saved for immunoblotting. The other 90% of samples
503 were separated by SDS-PAGE, visualized by colloidal coomassie blue staining,
504 destained and subjected to mass spectrometry (MS) analysis.

505 For MS analysis, the protein in the gel was subjected to trypsin digestion. In the LC-
506 MS/MS analysis, the digested products were separated using a 120-minute gradient
507 elution at a flow rate of 0.300 μL/min, utilizing the Thermo Ultimate 3000 nano-UPLC

508 system directly interfaced with the Thermo Fusion LUMOS mass spectrometer. The
509 analytical column used was an Acclaim PepMap RSLC (75 μm ID, 250 mm length,
510 C18). Mobile phase A consisted of 0.1% formic acid, while mobile phase B was 100%
511 acetonitrile with 0.1% formic acid. The Fusion LUMOS mass spectrometer operated in
512 data-dependent acquisition mode, employing Xcalibur 4.1.50 software. It started with
513 a single full-scan mass spectrum in the Orbitrap (375-1500 m/z, 60,000 resolution),
514 followed by data-dependent MS/MS scans. The MS/MS spectra from each LC-MS/MS
515 run were analyzed against the selected database using Proteome Discovery software
516 (version 2.4).
517
518 **Recombinant protein expression and GST pull-down assay**
519 For the expression of Glutathione S-transferase (GST) fusion proteins, GST-tagged
520 recombinant vectors were transfected into *Escherichia coli* Rosetta (DE3) cells. Upon
521 the cell culture attaining an OD_{600} between 0.6 and 0.8, the cells were subjected to
522 overnight incubation with 1 mM isopropyl-β-D-thiogalactopyranoside (IPTG; Sigma,
523 #92320) at 20°C. For the purification of GST fusion proteins, cells were collected and
524 sonicated.
525 For GST-pull down assays, HEK293T cells were transfected and subsequently lysed
526 on ice for over 15 minutes. Purified GST or GST fusion proteins were anchored onto
527 Glutathione Sepharose 4B beads (Pharmacia Biotech). These beads were then further
528 incubated with cellular extract at 4°C for an extended period of over 4 hours, followed
529 by washes with ice-cold PBS for three times. The process concluded with Western blot
530 analysis.
531
532 **RNA extraction and qRT-PCR**
533 Total RNA was isolated using Trizol reagent (Invitrogen) as per the manufacturer's
534 guidelines. 1 μg of the isolated RNA was converted to cDNA using HiScript II Q RT
535 SuperMix for qPCR (+gDNA wiper) (Vazyme). Quantitative real-time PCR, carried out

536 in triplicate, was used to assess relative mRNA levels and was standardized to *GAPDH*
537 expression. The cDNA products were amplified using the LightCycler 96 (Roche)
538 platform, and data were subsequently analyzed through LightCycler 96 (Roche) along
539 with GraphPad Prism 7.0 software. All relevant primers are listed in Table S2.
540
541 **Histology and immunohistochemistry staining**
542 Tissues were preserved in 4% paraformaldehyde, embedded in paraffin, and then sliced
543 into 5 μm sections prior to staining. Following deparaffinization and rehydration, these
544 sections were subject to H&E staining for structural examination.
545 Immunohistochemistry staining was executed using the streptavidin-biotin-peroxidase
546 complex method, with subsequent detection of 3'3'-diaminobenzidine (DAB) as guided
547 by the manufacturer's instructions (Dako, Agilent pathology solutions). Observations
548 and imaging were performed using an Olympus BX51 microscope coupled with an
549 Olympus DP73 CCD photography system.
550
551 **Tumor tissue microarray (TMA) immunohistochemistry analysis**
552 Human breast carcinoma TMA (HBre-Duc140Sur-01) was purchased from Shanghai
553 Biochip. Immunohistochemistry staining for FRMD8 in TMA was performed as
554 described above. The stained microarrays were evaluated by a pathologist blind to
555 cancer outcomes. Based on histological evaluations, staining reactivity was categorized
556 into four levels: absence of reactivity (score=0), weak reactivity (score=1), moderate
557 reactivity (score=2), and intense reactivity (score=3 or 4).
558
559 **Multiple immunohistochemistry staining and analysis**
560 Multicolor immunohistochemistry was conducted using the TissueGnostics Multiple
561 IHC Assay Kit (TissueGnostics, TGFP550) on mammary tumors from mice. Tumors
562 were preserved in 4% paraformaldehyde, embedded in paraffin, and then sliced into 5
563 μm sections prior to staining. The sections were then deparaffinized and hydrated,

564 followed by antigen retrieval in a Tris-EDTA buffer via microwave. Slides underwent
565 treatment with 3% H_2O_2 at ambient temperature to eliminate endogenous peroxidase
566 activity. For iterative rounds of cyclic staining, slides were treated with blocking
567 solution, then incubated with the primary antibody either overnight at 4°C or for 2 hours
568 at 37°C, and subsequently with HRP-linked secondary antibody at 37°C for 30 minutes.
569 Signal was enhanced using Tyramide Signal Amplification (TSA) reagents. Antigen
570 retrieval buffer was applied once more, and the aforementioned steps were repeated for
571 additional staining. Lastly, DAPI was used for 10 minutes to stain nuclei. Tissue images
572 were captured using the tissue faxs platform (TissueGnostics).
573 Immunofluorescence image quantification was carried out via StrataQuest v7.0.158
574 software (TissueGnostics). Cells were identified based on DAPI staining, and the
575 expression levels of Frmd8, ERα, PR, and CK8 were calculated by the software,
576 measuring fluorescence intensity and area to enumerate positively-stained cells. The
577 threshold for identifying positive cells was set by inspecting cell recognition on the
578 original image using the View Backward Data function.
579
580 **EdU (5-ethynyl-2'-deoxyuridine) incorporation assay**
581 The EdU incorporation assay was performed according to the manufacturer's
582 instructions of BeyoClick™ EdU Cell Proliferation Kit with Alexa Fluor 488
583 (Beyotime Biotechnology, #C0071) for cell proliferation.
584
585 **Single-cell RNA sequence (scRNA-seq)**
586 Single-cell RNA sequencing libraries were meticulously prepared utilizing the
587 Chromium Single Cell 3' Reagent Kits v3 according to the protocols recommended by
588 10× Genomics. Briefly, an initial quantity of approximately 1×10^5 cells, which had
589 been sorted through fluorescence-activated cell sorting (FACS), underwent a triple
590 wash process in DPBS containing 0.04% BSA. These cells were subsequently
591 resuspended to a final concentration of 700 to 1,200 cells/μl, with a minimum viability

592 threshold of 85%. During the library preparation process, cells were encapsulated
593 within droplets to facilitate a precise targeted recovery rate. After the reverse
594 transcription phase, the generated emulsions were disrupted, and the barcoded cDNA
595 was isolated using Dynabeads technology. This was followed by PCR amplification to
596 enrich the cDNA pool. The amplified cDNA served as the template for constructing the
597 3' gene expression libraries. Specifically, for this construction phase, 50 ng of the
598 amplified cDNA was fragmented and subjected to end repair. This material was then
599 subjected to a double-size selection process using SPRIselect beads. The prepared
600 libraries were sequenced on NovaSeq system provided by Illumina, generating 150 bp
601 paired-end reads.
602
603 **Single-cell RNA sequence original data process**
604 Prior to commencing the analysis, cellular data underwent a stringent filtering process.
605 Cells with unique molecular identifier (UMI) counts below 30,000 and those exhibiting
606 gene counts within the range of 200 to 5,000 were excluded. Additionally, cells
607 displaying a mitochondrial content exceeding 20% were also removed from further
608 analysis. Following this preprocessing step, the Seurat package (version 2.3) was
609 employed for both dimensionality reduction and cluster identification. The
610 normalization and scaling of gene expression data were accomplished using the
611 NormalizeData and ScaleData functions, respectively. Subsequently, the
612 FindVariableFeatures function facilitated the selection of the 2,000 genes
613 demonstrating the most significant variation for principal component analysis (PCA).
614 Cluster identification was achieved through the FindClusters function, which
615 partitioned the genes into distinct groups. To mitigate batch effects across samples, the
616 Harmony package was utilized. The refined dataset was then visualized in a two-
617 dimensional space employing Uniform Manifold Approximation and Projection
618 (UMAP) techniques, thereby providing insightful representations of the underlying
619 cellular heterogeneity.

620

621 **Chromosomal copy-number variations estimation**

622 The estimation of chromosomal copy-number variations (CNVs) was conducted
623 utilizing the 'inferCNV' R package. A diverse reference panel comprised of B cells, T
624 cells, NK cells, macrophages and other immune cells facilitated this analysis.
625 Quantification of CNV scores for each subcluster was achieved by aggregating the
626 CNV levels observed across the constituent cells.

627

628 **Quantification and statistical analysis**

629 Statistical comparisons were performed using unpaired two-tailed Student's t tests,
630 Mann Whitney test, one-way ANOVA or two-way ANOVA. Statistical analyses were
631 performed using GraphPad Prism 9.0 software (GraphPad Software, La Jolla, CA,
632 USA). Data are presented as mean ± the standard error of the mean (SEM). Statistical
633 significance was defined as $p<0.05$.

634

Data Availability

The accession number for the scRNA-seq data reported in this paper is Gene Expression Omnibus (GEO): GSE244582.

Conflict of Interest Statement

The authors have no potential conflicts of interest.

Acknowledgments

This study was supported by grants from the Ministry of Science and Technology of China 2022YFA1104003 and 2021YFC2501000; National Natural Science Foundation of China grants 82172972, 82230094, 81972616, 81972609 and 81772840; Peking University Medicine Sailing Program for Young Scholars' Scientific & Technological Innovation BMU2024YFJHPY004; the Fundamental Research Funds for the Central Universities; Postdoctoral Fellowship Program of CPSF GZC20230159. We would like to thank TissueGnostics Aisa Pacific Limited for their technical support on multiple immunohistochemistry staining.

Corresponding Authors

Correspondence to Hongquan Zhang or Jun Zhan.

References

Arden, K. C. (2004). FoxO: linking new signaling pathways. *Mol Cell*, *14*(4), 416-418. https://doi.org/10.1016/s1097-2765(04)00213-8

Badenes, M., Burbridge, E., Oikonomidi, I., Amin, A., de Carvalho, É., Kosack, L., Mariano, C., Domingos, P., Faísca, P., & Adrain, C. (2023). The ADAM17 sheddase complex regulator iTAP/Frmd8 modulates inflammation and tumor growth. *Life Science Alliance*, *6*(4). https://doi.org/10.26508/lsa.202201644

Badia, E., Oliva, J., Balaguer, P., & Cavaillès, V. (2007). Tamoxifen resistance and epigenetic modifications in breast cancer cell lines [Review]. *Current Medicinal Chemistry*, *14*(28), 3035-3043. https://doi.org/10.2174/092986707782794023

Frame, M. C., Patel, H., Serrels, B., Lietha, D., & Eck, M. J. (2010). The FERM domain: organizing the structure and function of FAK. *Nat Rev Mol Cell Biol*, *11*(11), 802-814. https://doi.org/10.1038/nrm2996

Habara, M., & Shimada, M. (2022). Estrogen receptor alpha revised: Expression, structure, function, and stability. *Bioessays*, *44*(12), e2200148. https://doi.org/10.1002/bies.202200148

Harbeck, N., Penault-Llorca, F., Cortes, J., Gnant, M., Houssami, N., Poortmans, P., Ruddy, K., Tsang, J., & Cardoso, F. (2019). Breast cancer. *Nat Rev Dis Primers*, *5*(1), 66. https://doi.org/10.1038/s41572-019-0111-2

Jia, X., Li, C., Li, L., Liu, X., Zhou, L., Zhang, W., Ni, S., Lu, Y., Chen, L., Jeong, L. S., Yu, J., Zhang, Y., Zhang, J., He, S., Hu, X., Sun, H., Yu, K., Liu, G., Zhao, H.,…Shao, Z. M. (2019). Neddylation Inactivation Facilitates FOXO3a Nuclear Export to Suppress Estrogen Receptor Transcription and Improve Fulvestrant Sensitivity. *Clin Cancer Res*, *25*(12), 3658-3672. https://doi.org/10.1158/1078-0432.Ccr-18-2434

Katzenellenbogen, J. A., Mayne, C. G., Katzenellenbogen, B. S., Greene, G. L., & Chandarlapaty, S. (2018). Structural underpinnings of oestrogen receptor mutations in endocrine therapy resistance. *Nature Reviews Cancer*, *18*(6), 377-388. https://doi.org/10.1038/s41568-018-0001-z

Koš, M., Reid, G., Denger, S., & Gannon, F. (2001). Minireview: Genomic Organization of the Human ERα Gene Promoter Region. *Molecular Endocrinology*, *15*(12), 2057-2063. https://doi.org/10.1210/mend.15.12.0731

Künzel, U., Grieve, A. G., Meng, Y., Sieber, B., Cowley, S. A., & Freeman, M. (2018). FRMD8 promotes inflammatory and growth factor signalling by stabilising the iRhom/ADAM17 sheddase complex. *eLife*, *7*, e35012. https://doi.org/10.7554/eLife.35012

Lapidus, R. G., Nass, S. J., & Davidson, N. E. (1998). The loss of estrogen and progesterone receptor gene expression in human breast cancer. *J Mammary Gland Biol Neoplasia*, *3*(1), 85-94. https://doi.org/10.1023/a:1018778403001

Légaré, S., & Basik, M. (2016). Minireview: The link between ERα corepressors and histone deacetylases in tamoxifen resistance in breast cancer [Review]. *Molecular Endocrinology*, *30*(9), 965-976. https://doi.org/10.1210/me.2016-1072

Liu, H., Song, Y., Qiu, H., Liu, Y., Luo, K., Yi, Y., Jiang, G., Lu, M., Zhang, Z., Yin, J., Zeng, S., Chen, X., Deng, M., Jia, X., Gu, Y., Chen, D., Zheng, G., & He, Z. (2020). Downregulation of FOXO3a by DNMT1 promotes breast cancer stem cell properties and tumorigenesis. *Cell Death & Differentiation*, *27*(3), 966-983. https://doi.org/10.1038/s41418-019-0389-3

Moleirinho, S., Tilston-Lunel, A., Angus, L., Gunn-Moore, F., & Reynolds, P. A. (2013). The expanding family of FERM proteins. *Biochem J*, *452*(2), 183-193. https://doi.org/10.1042/BJ20121642

Oikonomidi, I., Burbridge, E., Cavadas, M., Sullivan, G., Collis, B., Naegele, H., Clancy, D., Brezinova, J., Hu, T., Bileck, A., Gerner, C., Bolado, A., von Kriegsheim, A., Martin, S. J., Steinberg, F., Strisovsky, K., & Adrain, C. (2018). iTAP, a novel iRhom interactor, controls TNF secretion by policing the stability of iRhom/TACE. *eLife*, *7*, e35032. https://doi.org/10.7554/eLife.35032

Rogatsky, I., Trowbridge, J. M., & Garabedian, M. J. (1999). Potentiation of Human Estrogen Receptor α Transcriptional Activation through Phosphorylation of Serines 104 and 106 by the Cyclin A-CDK2 Complex*. *Journal of Biological Chemistry*, *274*(32), 22296-22302. https://doi.org/https://doi.org/10.1074/jbc.274.32.22296

Rondón-Lagos, M., Villegas, V. E., Rangel, N., Sánchez, M. C., & Zaphiropoulos, P. G. (2016). Tamoxifen resistance: Emerging molecular targets [Review]. *International Journal of Molecular Sciences*, *17*(8), Article 1357. https://doi.org/10.3390/ijms17081357

Seoane, J., Le, H.-V., Shen, L., Anderson, S. A., & Massagué, J. (2004). Integration of Smad and Forkhead Pathways in the Control of Neuroepithelial and Glioblastoma Cell Proliferation. *Cell*, *117*(2), 211-223. https://doi.org/https://doi.org/10.1016/S0092-8674(04)00298-3

Sun, J., Zhou, W., Kaliappan, K., Nawaz, Z., & Slingerland, J. M. (2012). ERα phosphorylation at Y537 by Src triggers E6-AP-ERα binding, ERα ubiquitylation, promoter occupancy, and target gene expression. *Mol Endocrinol*, *26*(9), 1567-1577. https://doi.org/10.1210/me.2012-1140

Sung, H., Ferlay, J., Siegel, R. L., Laversanne, M., Soerjomataram, I., Jemal, A., & Bray, F. (2021). Global Cancer Statistics 2020: GLOBOCAN Estimates of Incidence and Mortality Worldwide for 36 Cancers in 185 Countries. *CA: A Cancer Journal for Clinicians*, *71*(3), 209-249. https://doi.org/https://doi.org/10.3322/caac.21660

Valdes-Mora, F., Salomon, R., Gloss, B. S., Law, A. M. K., Venhuizen, J., Castillo, L., Murphy, K. J., Magenau, A., Papanicolaou, M., Rodriguez de la Fuente, L., Roden, D. L., Colino-Sanguino, Y., Kikhtyak, Z., Farbehi, N., Conway, J. R. W., Sikta, N., Oakes, S. R., Cox, T. R., O'Donoghue, S. I.,…Gallego-Ortega, D. (2021). Single-cell transcriptomics reveals involution mimicry during the specification of the basal breast cancer subtype. *Cell Rep*, *35*(2), 108945. https://doi.org/10.1016/j.celrep.2021.108945

Waks, A. G., & Winer, E. P. (2019). Breast Cancer Treatment: A Review. *Jama*, *321*(3), 288-300. https://doi.org/10.1001/jama.2018.19323

Williams, C. C., Basu, A., El-Gharbawy, A., Carrier, L. M., Smith, C. L., & Rowan,

B. G. (2009). Identification of four novel phosphorylation sites in estrogen receptor α: impact on receptor-dependent gene expression and phosphorylation by protein kinase CK2. *BMC Biochemistry*, *10*(1), 36. https://doi.org/10.1186/1471-2091-10-36

Yan, H., Li, Q., Wu, J., Hu, W., Jiang, J., Shi, L., Yang, X., Zhu, D., Ji, M., & Wu, C. (2017). MiR-629 promotes human pancreatic cancer progression by targeting FOXO3. *Cell Death & Disease*, *8*(10), e3154-e3154. https://doi.org/10.1038/cddis.2017.525

Yu, M., Wu, W. J., Sun, Y., Yan, H. Y., Zhang, L., Wang, Z. B., Gong, Y. Q., Wang, T. Z., Li, Q. C., Song, J. G., Wang, M. Y., Zhang, J., Tang, Y., Zhan, J., & Zhang, H. Q. (2023). FRMD8 targets both CDK4 activation and RB degradation to suppress colon cancer growth. *Cell Reports*, *42*(8), 112886. https://doi.org/ARTN 112886

10.1016/j.celrep.2023.112886

Zhan, J., & Zhang, H. (2018). Kindlins: Roles in development and cancer progression. *Int J Biochem Cell Biol*, *98*, 93-103. https://doi.org/10.1016/j.biocel.2018.03.008

Zhou, W., & Slingerland, J. M. (2014). Links between oestrogen receptor activation and proteolysis: relevance to hormone-regulated cancer therapy. *Nature Reviews Cancer*, *14*(1), 26-38. https://doi.org/10.1038/nrc3622

Figure Legends

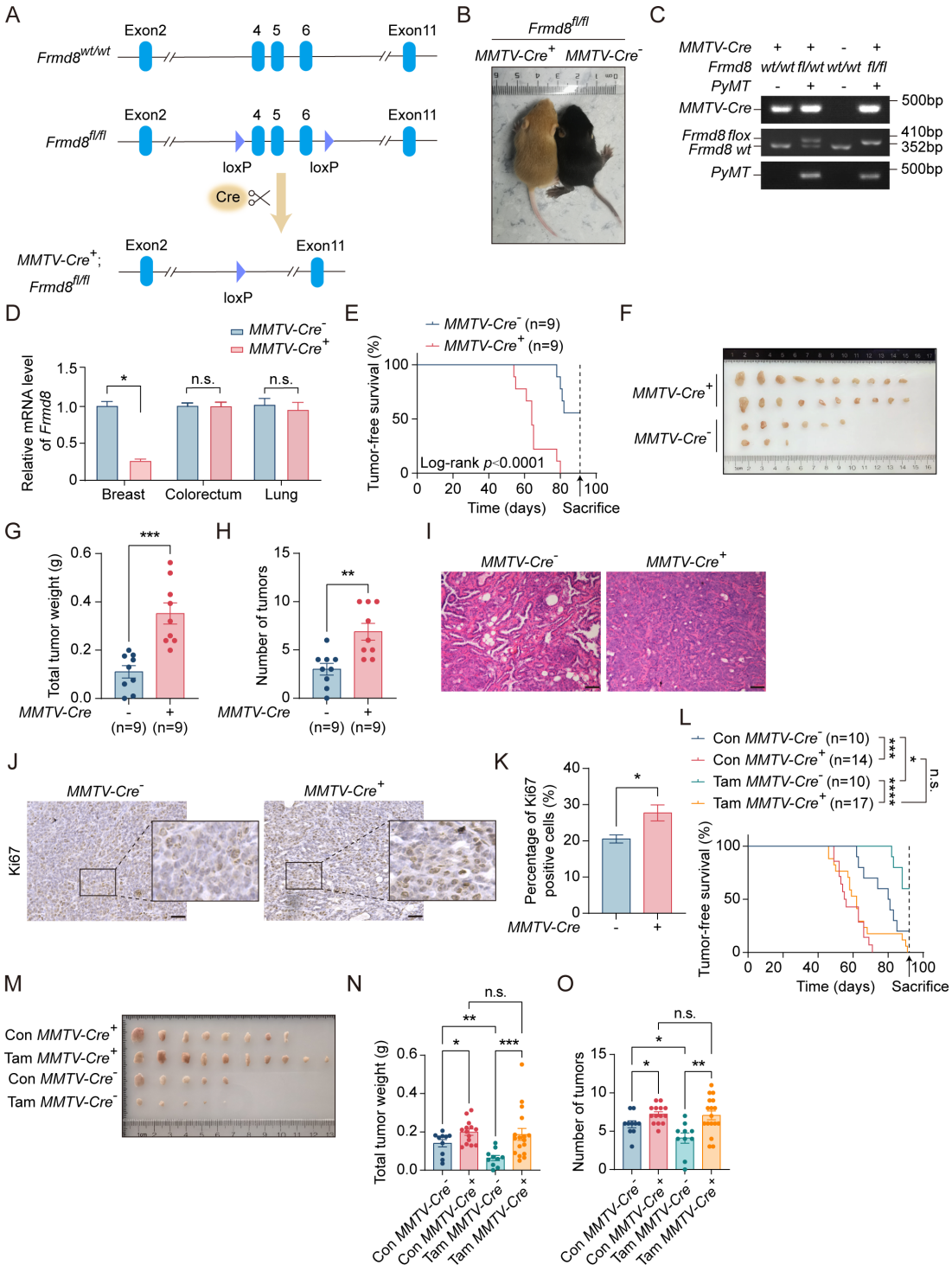

758 **Figure 1. Loss of Frmd8 promotes mammary tumor growth and generates**
759 **tamoxifen resistance *in vivo***
760 (A) A diagram of the *Frmd8* targeted alleles. Exons 4, 5 and 6 are flanked by loxp sites.
761 (B) Distinguishing the genotype of littermate mice by mice coat color. Yellow
762 represents *MMTV-Cre*$^{+}$; *Frmd8*$^{fl/fl}$; *PyMT* genotype and black represents *MMTV-Cre*$^{-}$;
763 *Frmd8*$^{fl/fl}$; *PyMT* genotype. (C) Representative PCR genotyping of mouse tail DNA. (D)
764 Relative mRNA level of *Frmd8* in 7-week-old mammary glands from *PyMT* mice was
765 analyzed by qRT-PCR. *Gapdh* was used as an internal reference. *p<0.05 by unpaired
766 Student's t-test. (E) Kaplan-Meier plot showing the appearance of palpable tumors in
767 *MMTV-Cre*$^{-}$; *Frmd8*$^{fl/fl}$; *PyMT* (n=9) and *MMTV-Cre*$^{+}$; *Frmd8*$^{fl/fl}$; *PyMT* (n=9) mice
768 (Log-rank test). (F) Representative images of tumors from *MMTV-Cre*$^{-}$; *Frmd8*$^{fl/fl}$;
769 *PyMT* and *MMTV-Cre*$^{+}$; *Frmd8*$^{fl/fl}$; *PyMT* mice. (G-H) Total tumor weight (G) and
770 number of tumors (H) per mice were measured. **p<0.01, ***p<0.001 by unpaired
771 Student's t-test. (I) Representative H&E staining of tumors from *MMTV-Cre*$^{-}$; *Frmd8*$^{fl/fl}$;
772 *PyMT* and *MMTV-Cre*$^{+}$; *Frmd8*$^{fl/fl}$; *PyMT* mice. Scale bar, 50 μm. (J)
773 Immunohistochemistry (IHC) staining for Ki67 expression in mammary tumors from
774 *PyMT* mice. The black boxes represent the magnified typical staining of the original
775 images. Scale bar, 50 μm. (K) Quantification of Ki67-positive cell percentage in (J).
776 *p<0.05 by unpaired Student's t-test. (L) Kaplan-Meier plot showing the appearance of
777 palpable tumors in *MMTV-Cre*$^{-}$; *Frmd8*$^{fl/fl}$; *PyMT* and *MMTV-Cre*$^{+}$; *Frmd8*$^{fl/fl}$; *PyMT*
778 mice, with or without tamoxifen treatment (Log-rank test, *p<0.05, ***p<0.001,
779 ****p<0.0001). (M) Representative images of tumors from *MMTV-Cre*$^{-}$; *Frmd8*$^{fl/fl}$;
780 *PyMT* and *MMTV-Cre*$^{+}$; *Frmd8*$^{fl/fl}$; *PyMT* mice, with or without tamoxifen treatment.
781 (N-O) Total tumor weight (N) and number of tumors (O) per mice from (L) were
782 measured. *p<0.05, **p<0.01, ***p<0.001 by unpaired Student's t-test or Mann
783 Whitney test.
784

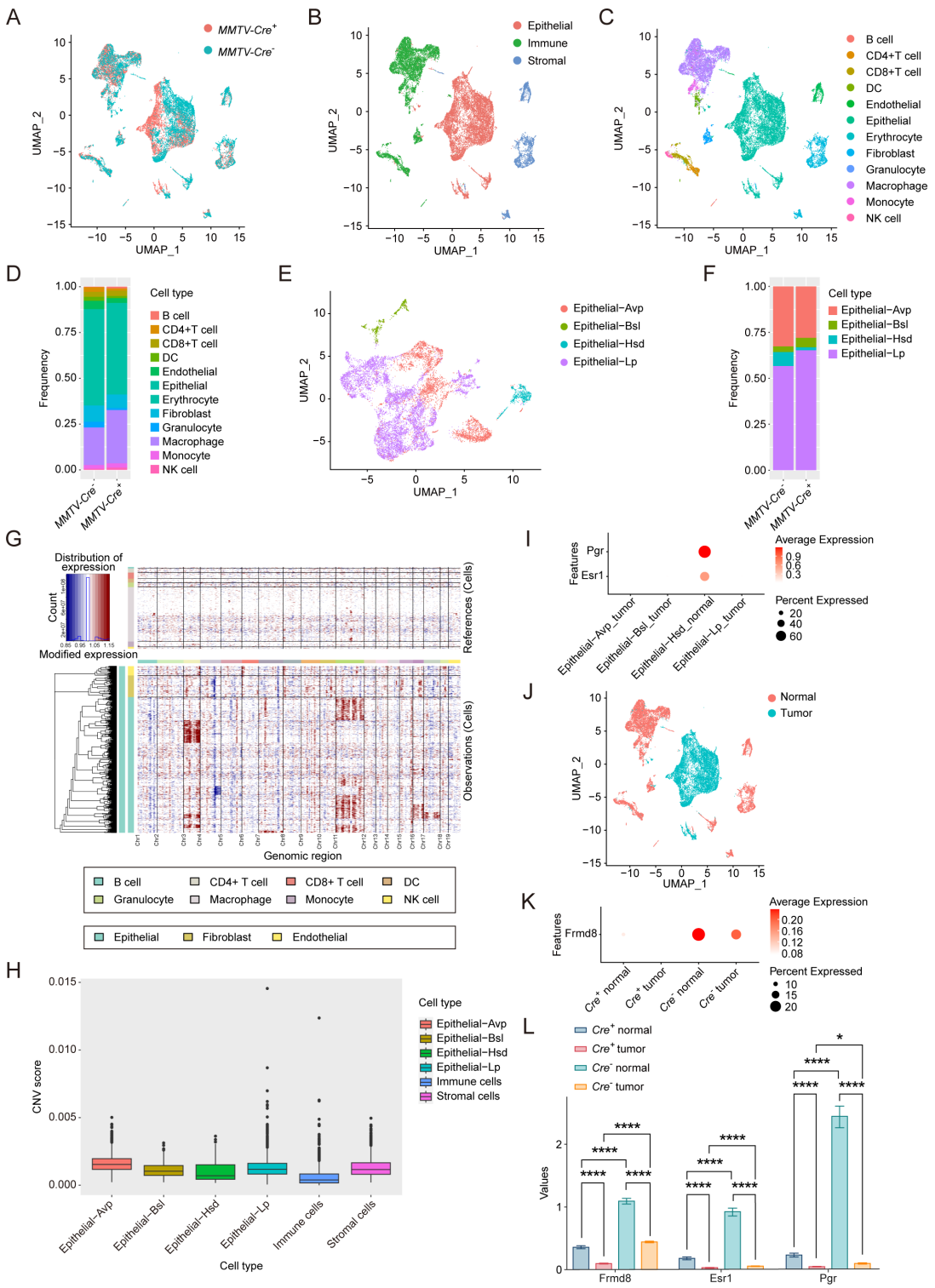

Figure 2. Frmd8 knockout decreases the proportion of the hormone-sensing differentiated epithelial cells

(A) T-SNE plot showing the distribution of cells from *MMTV-Cre*$^{-}$; *Frmd8*$^{fl/fl}$; *PyMT* and *MMTV-Cre*$^{+}$; *Frmd8*$^{fl/fl}$; *PyMT* mice. (B) T-SNE plot showing the distribution of

epithelial, immune and stromal cells. (C-D) T-SNE plot showing the distribution of main cell linages (C) and their relative percentage (D). (E-F) T-SNE plot showing the distribution of epithelial cell linages (E) and their relative percentage (F). (G) Heatmap showing distinct features of each cell lineages. Rows, genes. Columns, cells. The color key from blue to red indicates low to high gene expression. (H) Boxplot showing CNV score of main cell linages. (I) Dot plot showing the expression of *Esr1* and *Pgr* in epithelial cell linages. (J) T-SNE plot showing the distribution of normal cells and tumor cells. (K) Dot plot showing the expression of *Frmd8* in normal and tumor cells from *MMTV-Cre*$^{-}$; *Frmd8*$^{fl/fl}$; *PyMT* and *MMTV-Cre*$^{+}$; *Frmd8*$^{fl/fl}$; *PyMT* mice. (L) Statistical analysis of *Frmd8*, *Esr1* and *Pgr* expression in normal and tumor cells from *MMTV-Cre*$^{-}$; *Frmd8*$^{fl/fl}$; *PyMT* and *MMTV-Cre*$^{+}$; *Frmd8*$^{fl/fl}$; *PyMT* mice. *$p<0.05$, ****$p<0.0001$ by Mann-Whitney test.

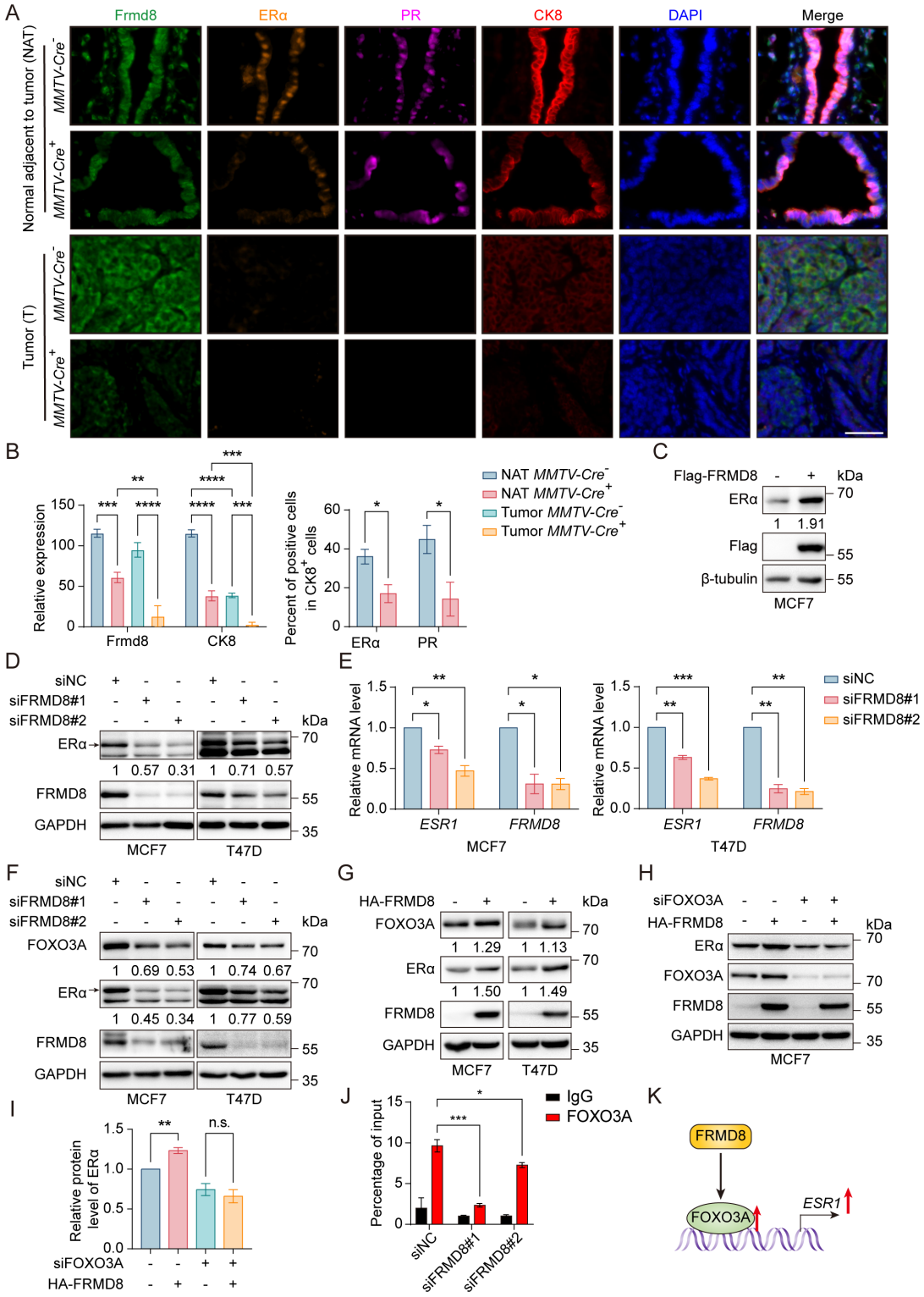

Figure 3. FRMD8 promotion of *ESR1* expression is mediated by FOXO3A

(A) Representative multiplex immunofluorescence images of tumor tissues and tissues adjacent to tumor from *MMTV-Cre*$^{-}$; *Frmd8*$^{fl/fl}$; *PyMT* and *MMTV-Cre*$^{+}$; *Frmd8*$^{fl/fl}$; *PyMT* mice. Scale bar, 50 μm. (B) Qualification of Frmd8 and CK8 expression (left

808 panel) and ERα and PR-positive cell percentage in $CK8^+$ cells (right panel) in (A).
809 *p<0.05, **p<0.01, ***p<0.001, ****p<0.0001 by one-way ANOVA (left panel) or
810 unpaired Student's t-test (right panel). (C) Lysates from MCF7 cells transiently
811 transfected with Flag or Flag-FRMD8 were immunoblotted. (D) Lysates from MCF7
812 and T47D cells transiently transfected with control or FRMD8 siRNA were
813 immunoblotted. In this and subsequent figures, specific bands are marked with an arrow.
814 (E) Relative mRNA levels of *ESR1* and *FRMD8* from MCF7 and T47D cells transiently
815 transfected with control or FRMD8 siRNA were analyzed by qRT-PCR. *GAPDH* was
816 used as an internal reference. *p<0.05, **p<0.01, ***p<0.001 by one-way ANOVA.
817 (F) Lysates from MCF7 and T47D cells transiently transfected with control or FRMD8
818 siRNA were immunoblotted. (G) Lysates from MCF7 and T47D cells transiently
819 transfected with HA or HA-FRMD8 were immunoblotted. (H-I) Lysates of MCF7 cells
820 co-transfected with HA-FRMD8 and FOXO3A siRNA as indicated were
821 immunoblotted (H). ERα protein levels were quantified by normalizing to the intensity
822 of the GAPDH band (I). **p<0.01 by unpaired Student's t-test. (J) Lysates of T47D
823 cells transfected with control or FRMD8 siRNA were subjected to anti-FOXO3A ChIP-
824 qPCR. *p<0.05, ***p<0.001 by one-way ANOVA. (K)Working model for FRMD8
825 promotes *ESR1* transcription via upregulating FOXO3A expression.
826

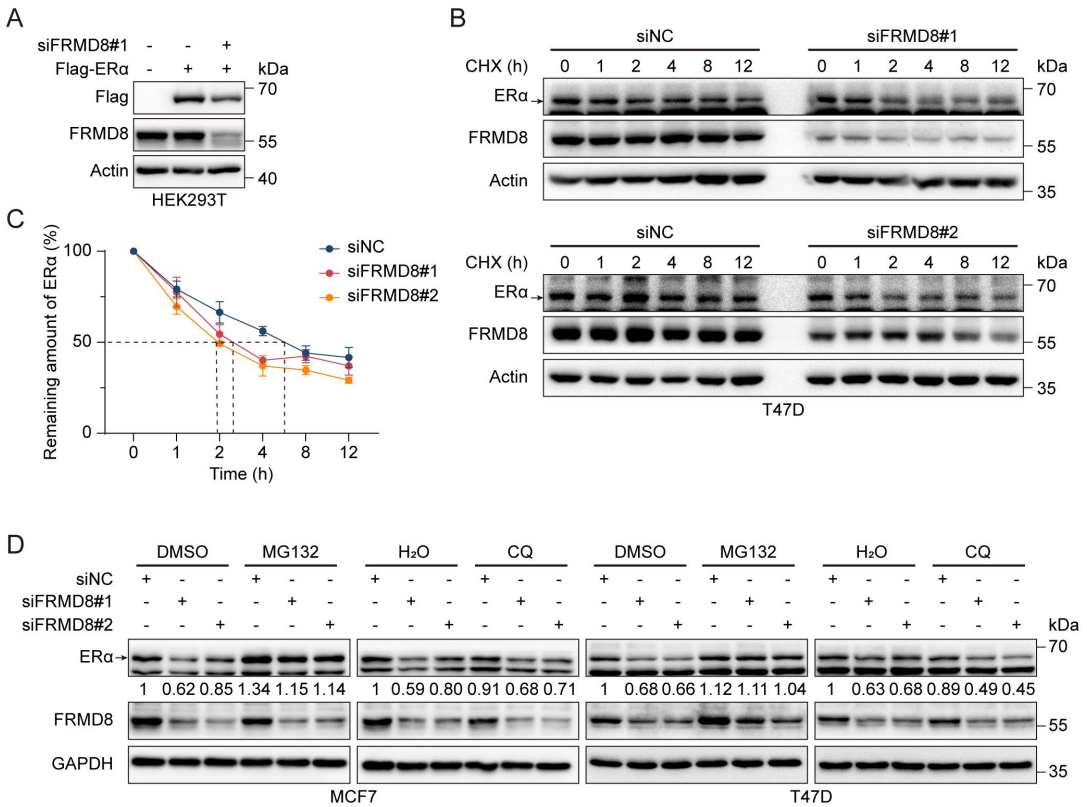

Figure 4. FRMD8 stabilizes ERα via prevention of its degradation

(A) Lysates of HEK293T cells co-transfected with Flag-ERα and FRMD8 siRNA as indicated were immunoblotted. (B-C) Lysates from T47D cells transiently transfected with control or FRMD8 siRNA were subjected to immunoblotting. Cells were treated with 100 μg/ml CHX for the indicated times (B). ERα protein levels were quantified by normalizing to the intensity of the Actin band (C). (D) Immunoblot analysis of ERα in MCF7 (D) and T47D (E) cells transiently transfected with control or FRMD8 siRNA. The cells were treated with MG132 (25 μM) or chloroquine (50 μM) for 6 h.

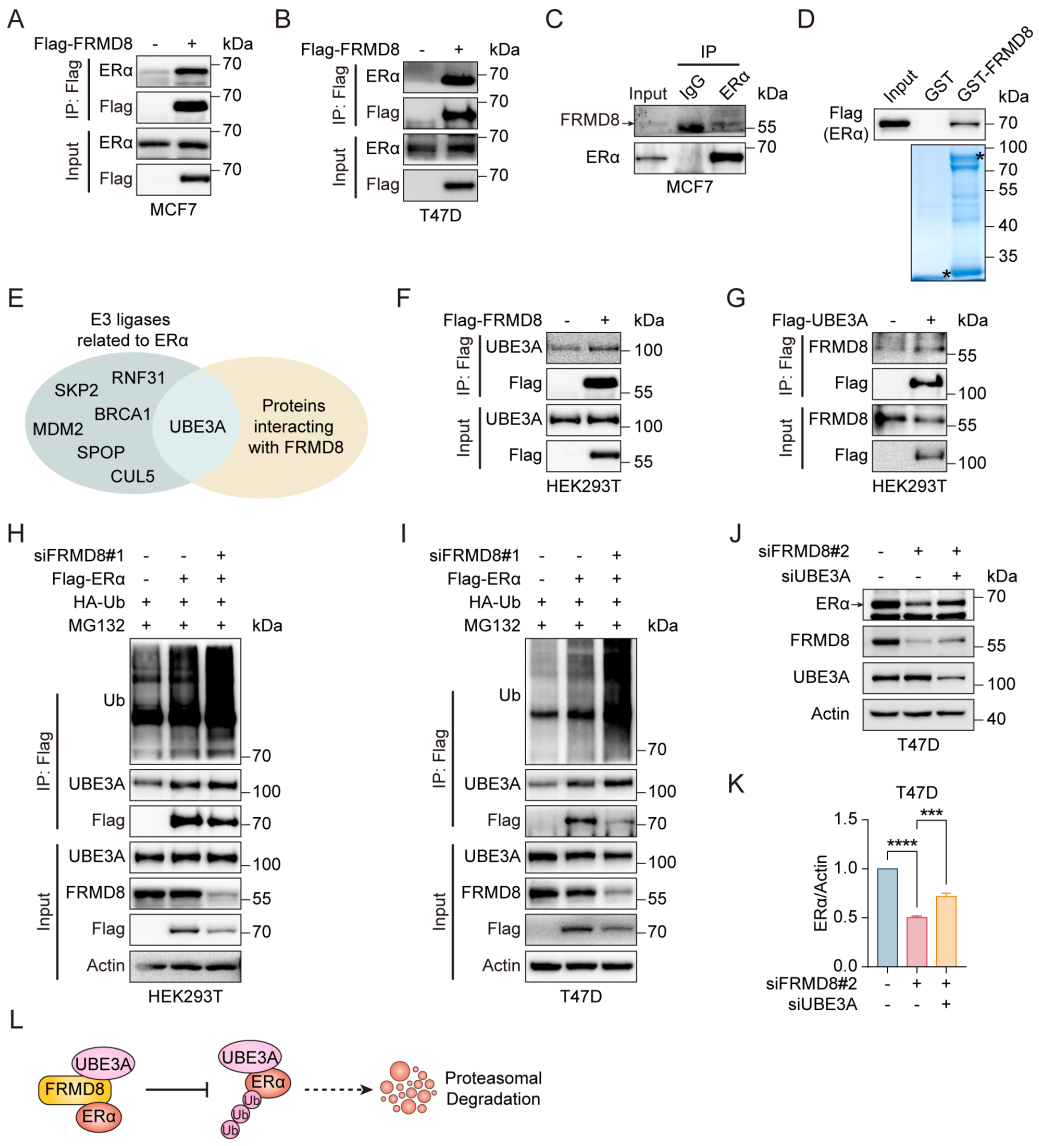

Figure 5. FRMD8 inhibits ERα degradation by blocking UBE3A binding with ERα

(A-B) Lysates of MCF7 (A) and T47D (B) cells transfected with Flag or Flag-FRMD8 were anti-Flag immunoprecipitated and immunoblotted for ERα and Flag. (C) Lysates from MCF7 cells were immunoprecipitated with IgG or anti-ERα, then immunoblotted for FRMD8 and ERα. (D) HEK293T cells were transiently transfected with Flag-ERα. ERα proteins in HEK293T whole cell lysates (WCL) pulled down by GST or GST-FRMD8 recombinant proteins were subjected to Western blot. Asterisks indicate proteins at the expected molecular weight. (E) Venn diagram showing overlap of E3 ligases related to ERα and proteins interacting with FRMD8. (F) Lysates of HEK293T cells transfected with Flag or Flag-FRMD8 were anti-Flag immunoprecipitated and

848 immunoblotted. (G) Lysates of HEK293T cells transfected with Flag or Flag-UBE3A
849 were anti-Flag immunoprecipitated and immunoblotted. (H-I) HEK293T (H) and T47D
850 (I) cells were co-transfected with Flag-ERα, HA-Ub and FRMD8 siRNA as indicated.
851 Cells were treated with MG132 (25 μM) for 6 h. WCL were immunoprecipitated with
852 anti-Flag and then immunoblotted for ubiquitinated ERα. (J-K) Lysates of T47D cells
853 co-transfected with FRMD8 and UBE3A siRNA as indicated were immunoblotted (J).
854 ERα protein levels were quantified by normalizing to the intensity of the Actin band
855 (K). ***$p<0.001$, ****$p<0.0001$ by one-way ANOVA. (L) Working model for FRMD8
856 disrupts the interaction between ERα and UBE3A, and protects ERα from UBE3A-
857 mediated degradation.
858

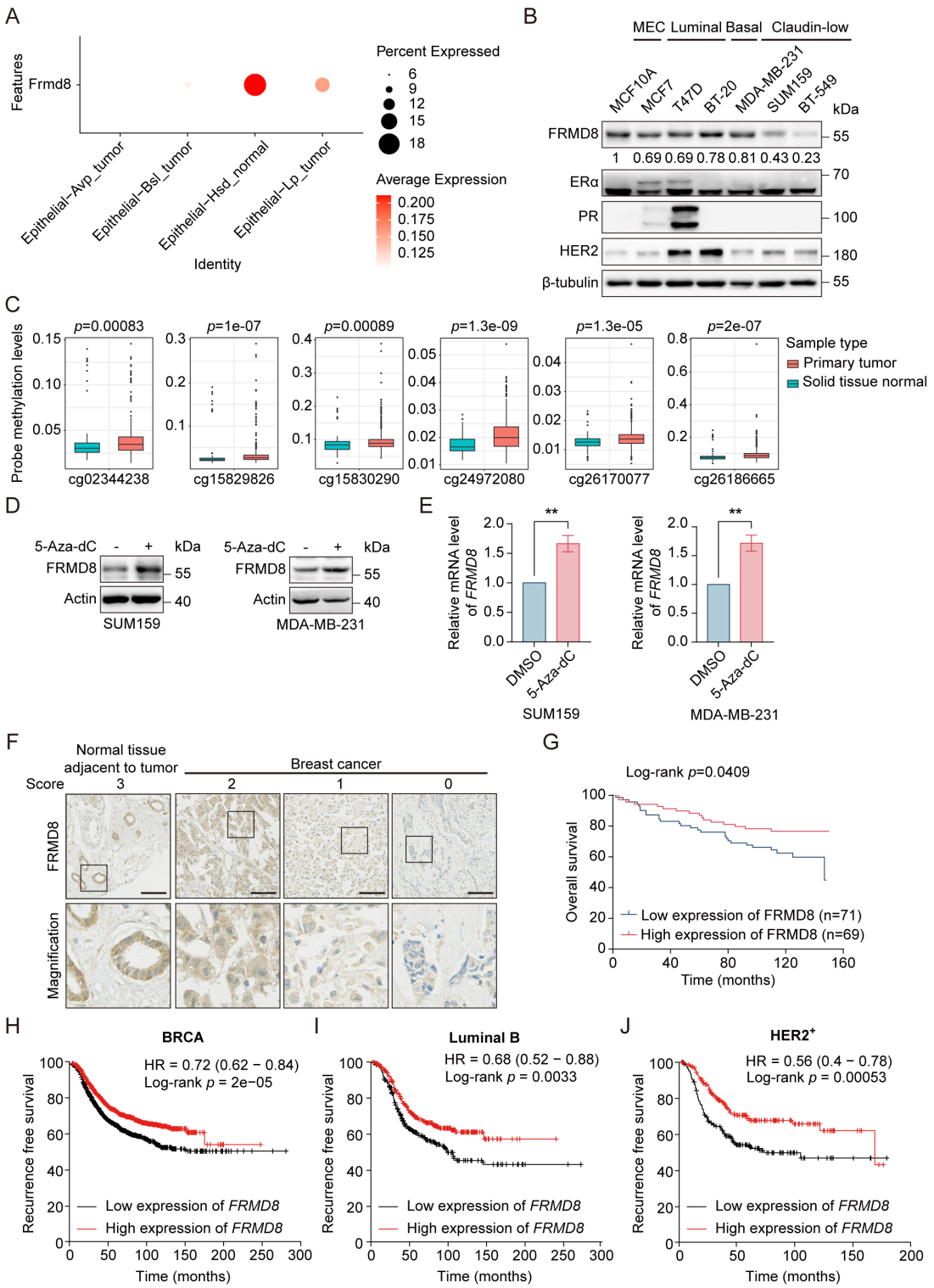

Figure 6. *FRMD8* promoter is methylated and low FRMD8 level predicts poor prognosis in breast cancer patients

(A) Dot plot showing the expression of *Frmd8* in epithelial cell linages from *PyMT* mice. (B) Lysates from human mammary epithelial cell (MEC) and breast cancer cells

were subjected to immunoblotting. (C) Methylation of *FRMD8* promoter region in breast cancer according to the University of California Santa Cruz (UCSC) database (http://xena.ucsc.edu/). (D) SUM159 and MDA-MB-231 cells were treated with 5-Aza-dC (10 μM) for 48 h. Protein expression of FRMD8 was examined by Western blot. (E) SUM159 and MDA-MB-231 cells were treated with 5-Aza-dC (10 μM) for 48 h. *FRMD8* mRNA levels was examined by quantitative reverse transcription PCR (qRT-PCR) *GAPDH* was used as an internal reference. $^{**}p<0.01$ by unpaired Student's t-test. (F) IHC analysis of FRMD8 expression in human breast carcinoma TMA was performed. Representative examples (scale bar, 100 μm) of normal tissue adjacent to tumor and breast cancer with different levels of FRMD8 expression are shown, with the magnification of selected areas inserted. (G) Kaplan-Meier analysis for the overall survival of breast cancer patients according to FRMD8 expression (Log-rank test). (H-J) Recurrence free survival of breast cancer patients according to *FRMD8* expression were analyzed according to Kaplan-Meier plotter (http://kmplot.com/analysis/).

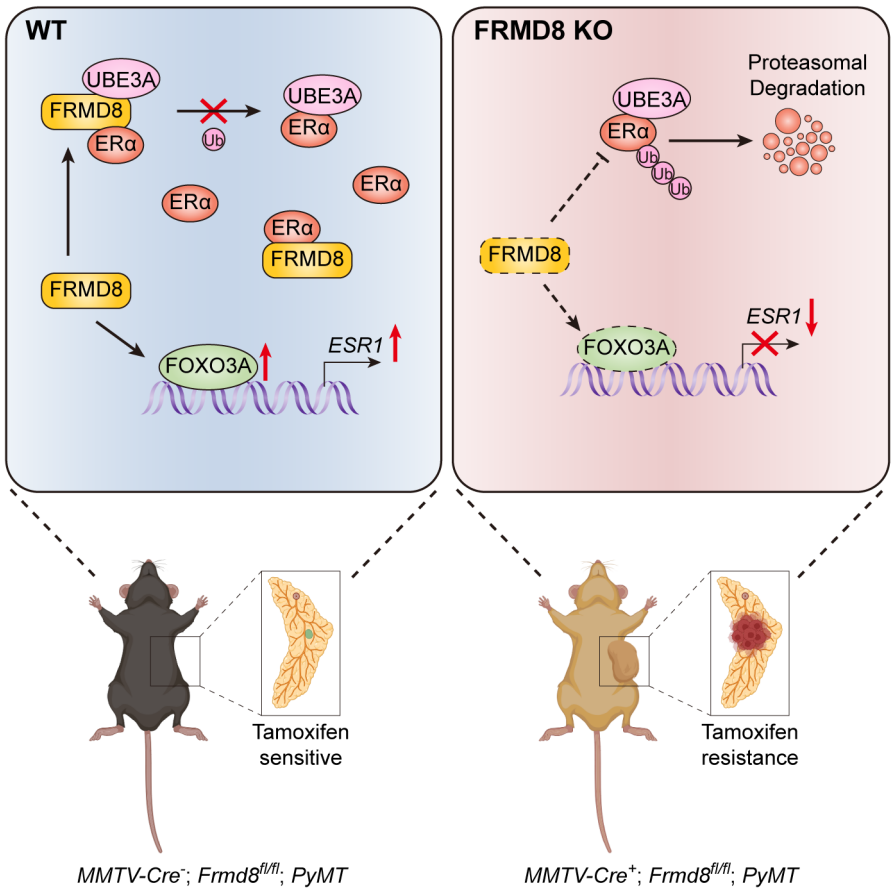

Figure 7. A working model shows that loss of FRMD8 promotes mammary tumor progression and confers tamoxifen resistance by downregulating ERα expression at both transcriptional and post-translational levels.